Quaternary Science Reviews
July 2017, Volume 167 Pages 1-13
https://doi.org/10.1016/j.quascirev.2017.04.020
https://archimer.ifremer.fr/doc/00384/49562/

Archimer
https://archimer.ifremer.fr

Age and duration of Laschamp and Iceland Basin geomagnetic excursions in the South Atlantic Ocean

Channell J. E. T. [1,*], Riveiros N. Vazquez [2,3], Gottschalk J. [3,4,5], Waelbroeck C. [2], Skinner L. C. [3]

[1] Univ Florida, Dept Geol Sci, POB 112120, Gainesville, FL 32611 USA.
[2] Univ Paris Saclay, LSCE, IPSL, CNRS,CEA,UVSQ, F-91198 Gif Sur Yvette, France.
[3] Univ Cambridge, Dept Earth Sci, Godwin Lab Palaeoclimate Res, Cambridge CB2 3EQ, England.
[4] Univ Bern, Inst Geol Sci, Baltzerstr 1 3, CH-3012 Bern, Switzerland.
[5] Univ Bern, Oeschger Ctr Climate Change Res, Baltzerstr 1 3, CH-3012 Bern, Switzerland.

* Corresponding author : J. E. T. Channell, email address : jetc@ufl.edu

Abstract :

Age models for new records of the Laschamp and Iceland Basin excursions from the eastern flank of the South Atlantic mid-ocean ridge (44.15°S, 14.22°W) are derived from radiocarbon dates, and from matching sea-surface temperature records to Antarctic (EPICA) air-temperature records from ice cores. The onset of the Laschamp excursion occurred during Antarctic Isotopic Maximum (AIM) 10, consistent with its occurrence during Greenland Interstadial 10. The end of the Laschamp excursion occurred prior to AIM 9 in Greenland Stadial 10. The age model is supported by synchroneity of directional and relative paleointensity manifestations of the Laschamp excursion in the marine core with peaks in EPICA10Be and nitrate flux. The Iceland Basin excursion is synchronous with the final phase of the transition from marine isotope stage (MIS) 7a to MIS 6e as recorded in the EPICA δD record. The onset of the Laschamp and Iceland Basin excursions, defined here by component inclinations >−40°, occurred at 41.4 ka and 190.0 ka, and durations are ~1 kyr and ~3.5 kyr, respectively, although these estimates depend on the criteria used to define the directional excursions. By comparison with Laschamp and Iceland Basin excursion records from the North Atlantic Ocean, the two excursions are synchronous at centennial timescales between the two hemispheres, based on synchronization of the GICC05 and AICC2012 age models for Greenland and Antarctic ice cores.

Highlights

► Rare recording of Laschamp and Iceland Basin excursions in the South Atlantic. ► Age model links excursions to Antarctic ice core and cosmogenic nuclide flux. ► South Atlantic ages consistent with North Atlantic ages for the excursions. ► No evidence of global diachroneity of magnetic excursions. ► Estimated mid-point ages (durations) are 40.9 ka (1 kyr) and 188 kyr (3.5 kyr).

Please note that this is an author-produced PDF of an article accepted for publication following peer review. The definitive publisher-authenticated version is available on the publisher Web site.

1. Introduction

Documenting the spatial distribution of magnetic excursion records, and determining their timing and duration, are important not only for gauging the usefulness of excursions in high-resolution stratigraphy but also for understanding the workings of the geodynamo. The proposal that the age of the Laschamp excursion, and its associated relative paleointensity (RPI) minimum, is location dependent (Leonhardt et al., 2009), and that the Matuyama-Brunhes (M-B) boundary is asynchronous from the Atlantic to the Pacific by ~10 kyr (Leonhardt and Fabian, 2007), have important implications for magnetic stratigraphy. Most Quaternary magnetic excursion and RPI records are from north of 35°N in the North Atlantic Ocean. Southern hemisphere records of the Laschamp excursion have been reported from several piston cores from the vicinity of the South Atlantic Agulhas Ridge (Fig. 1, Channell et al., 2000), from two piston cores from the Scotia Sea (Collins et al., 2012), from a single Indian Ocean core (MD94-

103) collected east of the Kerguelen Plateau (Mazaud et al., 2002), and from several sites occupied during Ocean Drilling Program (ODP) Leg 202, principally Site 1233 at 41.0°S, 74.26°W, off southern Chile (Lund et al., 2006a,b; Stoner et al., 2008). The only southern hemisphere record of the Iceland Basin excursion is from ODP Site 1089, again from the Agulhas Ridge (Fig. 1, Stoner et al., 2003).

Age models for the Agulhas Ridge records of the Laschamp and Iceland Basin excursions were based on benthic oxygen isotopes (Channell et al., 2000; Hodell et al., 2001; Mortyn et al., 2003) and their correlation to nearby Core RC11-83, which has 14 radiocarbon ages in the 11-41 ka interval (Charles et al., 1996). The age models for the Scotia Sea Laschamp records (Collins et al., 2012) were derived by RPI correlation to the South Atlantic (SAPIS) paleointensity stack (Stoner et al., 2002). Similarly, the age model for the Indian Ocean record (Mazaud et al., 2002) was based on correlation of RPI proxies to the North Atlantic (NAPIS) RPI stack (Laj et al., 2000). Finally, the age model for the ODP Site 1233 (Lamy et al., 2004) was determined by correlation of alkenone sea-surface temperature (SST) data to the Byrd (Antarctic) ice core $\delta^{18}O$ record of Blunier and Brook (2001).

Here we report records of the Laschamp and Iceland Basin excursions from cores MD07-3076Q and MD07-3077, collected from *R/V Marion Dufresne* at a site (44.15°S, 14.22°W) on the eastern flank of the mid-Atlantic ridge at a water depth of 3770 m. The location is ~1985 km west of Agulhas Ridge (Fig. 1). Core MD07-3076Q is a 10.9-m square-section (25 x 25 cm) gravity core, and core MD07-3077 is a 49.5-m *Calypso* piston core that extends back through the last ~500 kyr. The top ~10-15 m of cores retrieved with the *Calypso* corer prior to 2016 are usually “oversampled” (stretched) by ~30-40% during recovery (see Skinner and McCave, 2003; Széréméta et al., 2004). For this reason, we used the top six sections (sections are usually 1.5-m in length) of core MD07-3076Q down to 8.20 meters below seafloor (mbsf), which is equivalent to 75 ka, and core sections 9 to 21 of core MD07-3077 that correspond to the 12 to 31 mbsf interval in this core. Below 31 mbsf (~250 ka), low magnetization intensities limit the fidelity of the records, so we restrict our discussion to the last 250 kyr. Blue reflectance data from the two cores (Fig. 2) indicate that the base of the studied interval in core MD07-3076Q (at 8.2 mbsf) corresponds to the 13.5 mbsf level in core MD07-3077 due to core stretching in the upper part of core MD07-3077.

The new South Atlantic records of the Laschamp and Iceland Basin excursions are notable, not only because southern hemisphere excursion records are rare, but also because of their relatively enhanced age control based on calibrated radiocarbon ages and on correlation of sea surface temperature proxies to the EPICA Dome C (EDC) δD record. The age control enables us to link the South Atlantic records of the two excursions to Antarctic (and Greenland) ice core chronologies, and hence to North Atlantic records of the same excursions, and to assess the global synchroneity of these magnetic excursions and their utility as stratigraphic markers.

2. Age Model

The age model for core MD07-3076Q back to 27 ka is based on 50 calibrated accelerator mass spectrometer (AMS) ^{14}C ages from monospecific planktic foraminifera, which are corrected for variable reservoir age effects based on alignment of variations in sea surface temperature to changes in Antarctic air-temperature from ice-core records (Skinner et al., 2010; Table 1; Fig. 2). Sea surface temperatures were reconstructed based on Mg/Ca ratios of planktic foraminifera *Globigerina bulloides* and *Neogloboquadrina pachyderma* (sin.), and on abundance variations of *N. pachyderma* (sin.) (Skinner et al., 2010; Vázquez Riveiros et al., 2010).

During marine isotope stage (MIS) 3, beyond 27 ka, the age model for core MD07-3076Q (Table 1, Fig. 2) is based on the stratigraphic alignment of abundance peaks of *G. bulloides* with Antarctic air-temperature maxima represented by minima in the EDC δD Antarctic ice-core record (Jouzel et al., 2007), transferred onto the AICC2012 age scale (Bazin et al., 2013; Veres et al., 2013). This age model (Table 1, Fig. 2) is consistent within 330 ±280 years with previously established chronologies for core MD07-3076Q (Gottschalk et al., 2015a,b).

A similar strategy was used for core MD07-3077 utilizing the alignment of abundance peaks of *G. bulloides* and abundance lows of *N. pachyderma* (sin.), with Antarctic air-temperature maxima represented by minima in the EDC δD Antarctic ice-core record (Fig. 2), following the procedure used for MIS 11 in the same core (Vázquez Riveiros et al., 2010; 2013). Two additional tie points for core MD07-3077, based on the correlation of maxima in planktic $\delta^{18}O$ with minima in Antarctic air-temperature, were added in MIS 4 (Table 2). Correlation between cores MD07-3076Q and MD07-3077 down to 13.5 mbsf (~100 ka) in MD07-3077 is based on blue reflectance data from each core (Fig. 2e), which permits the age model of MD07-3076Q to be transferred to MD07-3077, where the two cores overlap.

3. Natural Remanent Magnetization (NRM)

Continuous u-channel samples (2 x 2 x 150 cm^3 samples encased in plastic with a clip-on lid constituting one of the sides) were collected from slice B of the square-section gravity core MD07-3076Q (Sections 1-6) and from the archive halves of Sections 9-33 of calypso core MD07-3077. Sections 1-8 of core MD07-3077 were not sampled due to evidence for core stretching in the upper part of core MD07-3077, and because this part of the core was recovered in better condition in core MD07-3076Q. Measurements of the natural remanent magnetization

(NRM) of u-channel samples were made at 1-cm intervals, with a 10-cm leader and trailer at the top and base of each u-channel sample, using a 2-G Enterprises pass-through magnetometer at the University of Florida designed for the measurement of u-channel samples (Weeks et al., 1993; Guyodo et al., 2002). After initial NRM measurement of u-channel samples, stepwise alternating field (AF) demagnetization was carried out in 5 mT increments in the 10-60 mT peak field interval, and in 10 mT increments in the 60-100 mT interval, using tracking speeds of 10 cm/s. Component magnetizations were computed each 1-cm for a uniform 20-80 mT demagnetization interval (Fig. 3) following the standard least-squares method (Kirschvink, 1980) without anchoring to the origin of orthogonal projections, using UPmag software (Xuan and Channell, 2009). Maximum angular deviation (MAD) values are generally <10°, indicating moderately well-defined magnetization components apart from an interval close to the base of MD07-3076Q, and the lower half of MD07-3077 below ~35 mbsf (Fig. 3). Component declinations in Figure 3 are arbitrary and have not been adjusted for vertical-axis core rotation. The declination should, however, be uniform for the entire core because a consistent split-face for each core section was sampled. Twisting of sediment core is apparent in the declination record of core MD07-3077 (Fig. 3), particularly in the 25-35 mbsf (175-280 ka) interval. Although core twisting affects the component declinations, two magnetic excursions are apparent in the u-channel inclination and declination records at 4.06-4.36 mbsf in core MD07-3076Q, and at 26.48-27.00 mbsf in core MD07-3077 (Fig. 3). As will be discussed below, the former is a record of the Laschamp excursion (~41 ka) and the latter is a record of the Iceland Basin excursion (~188 ka). Below ~32 mbsf, MAD values increase as NRM intensities decrease (Fig. 3). We associate this decrease in magnetization intensity with magnetite dissolution associated with pore-water sulfate reduction. For this reason, data from below ~32 mbsf (250 ka) are not discussed further.

4. Laschamp and Iceland Basin excursions

Sedimentary records of the Laschamp excursion (~41 ka) are widely distributed in the North Atlantic Ocean and Gulf of Mexico (e.g., Laj et al., 2000, 2006; Lund et al., 2005; Channell, 2006; Evans et al., 2007; Channell et al., 2012), with additional records from the Black Sea (Nowaczyk et al., 2013), southern Indian Ocean (Mazaud et al., 2002), the Agulhas Ridge in the South Atlantic Ocean (Channell et al., 2000), Scotia Sea (Collins et al., 2012), and ODP Site 1233 off southern Chile (Lamy et al., 2004; Lund et al., 2006a,b; Stoner et al., 2008).

The Iceland Basin excursion (~190 ka) has been recorded repeatedly in sediments from the North Atlantic Ocean (e.g., Channell et al., 1997; Channell, 1999, 2006, 2014; Laj et al., 2006; Evans et al., 2007), the Pacific Ocean (e.g., Yamazaki and Ioka, 1994; Roberts et al., 1997; Laj et al., 2006), and from Lake Baikal (Oda et al., 2002). Until now, the only record of the Iceland Basin excursion reported from the southern hemisphere is from ODP Site 1089 from the Agulhas Ridge (Stoner et al., 2003).

NRM component directions from u-channel samples from cores MD07-3076Q and MD07-3077, although distorted by core twisting, indicate the presence of two magnetic excursions, at ~4 mbsf in core MD07-3776Q and at ~26.5 mbsf in core MD07-3077 (Fig. 3). The respective age models place the excursions at ~41 ka and ~190 ka, which indicates that they represent the Laschamp and Iceland Basin excursions, respectively. In order to confirm the presence of magnetic excursions in cores MD07-3076Q and MD07-3077, we collected cubic discrete (2 x 2 x 2 cm^3) samples back-to-back alongside the u-channel trough. Stepwise AF demagnetization of discrete samples resulted in magnetization components, calculated for a uniform 20-80 mT demagnetization interval, that indicate that the Laschamp and Iceland Basin excursions are recorded by both discrete and u-channel samples (Fig. 4). MAD values are, however, >10° for some discrete and u-channel measurements from the excursion intervals (Fig. 4), indicating poorly-defined magnetization components. A uniform 20-80 mT demagnetization interval for calculation of component magnetizations, for both discrete and u-channel samples, allows unambiguous assessment of data quality. Orthogonal projections of AF demagnetization data for discrete and u-channel samples that record the excursions often display well-defined magnetization components (Fig. 5), although component inclinations do not reach high positive values for either excursion, and the declination change for the Laschamp excursion is muted (Fig. 4). By comparison with numerous excursion records from the North Atlantic Ocean (e.g., Laj et al., 2006; Channell et al., 2012), the lack of antipodal directions from discrete and u-channel samples indicates that the NRM fidelity is compromised by magnetite dissolution. The median destructive field (MDF) of NRM increases abruptly from ~27 mT to ~45 mT in the 32-38 mbsf interval, implying the authigenic growth of high coercivity iron sulfides below ~35 mbsf.

5. Relative Paleointensity (RPI)

The intensity of detrital remanent magnetization (DRM) depends on the intensity of the geomagnetic field, and the concentration and alignment efficiency of remanence-carrying grains. The relative strength of the magnetizing field can be determined by using the intensity of different types of laboratory-induced magnetizations, including anhysteretic remanent magnetization (ARM) and isothermal remanent magnetization (IRM), to normalize the NRM intensity for changes in concentration of remanence-carrying grains. The normalizer should, therefore, activate the same grains that carry the NRM. The resulting normalized remanence can be used as a proxy for RPI variations if magnetite is the sole NRM carrier and occurs in a restricted grain-size range (Banerjee and Mellema, 1974; Levi and Banerjee, 1976; King et al., 1983; Tauxe, 1993).

After demagnetization and analysis of the NRM, ARM was imposed along the long-axis of u-channel samples in a peak AF of 100 mT and a DC bias field of 50 µT, and was then demagnetized at the same peak fields used to demagnetize the NRM. Subsequently, stepwise ARM acquisition was carried out using a uniform bias field (50 µT) and increasing values of peak AF (ARMAQ) at the same steps as for stepwise demagnetization. $IRM_{0.3T}$ was acquired using impulse fields of 0.3 T, and was demagnetized at the same peak fields as applied to the NRM and ARM, and then an additional IRM_{1T}, acquired in impulse fields of 1T, was demagnetized once more at the same peak demagnetization fields. This RPI protocol (Channell et al., 2002) allows us to calculate four RPI proxies as slopes: NRM/ARM, NRM/ARMAQ, NRM/ $IRM_{0.3T}$, and NRM/ IRM_{1T}; all calculated for the 20-60 mT demagnetization or acquisition interval using the UPmag software of Xuan and Channell (2009). Linear correlation coefficients (r) associated with each slope indicate that the slopes are well defined with r-values >0.98 (Fig. 6). The RPI proxies are essentially identical for NRM/ARM and NRM/ARMAQ (as expected), and for NRM/ $IRM_{0.3T}$, and NRM/ IRM_{1T}, but are different for NRM/ARM versus NRM/IRM particularly for 0-20 ka (Fig. 6). The RPI proxies can be partially matched to reference RPI records (Fig. 6) such as the South Atlantic paleointensity stack (SAPIS, Stoner et al., 2002), and to the global PISO paleointensity stack (Channell et al., 2009). There are, however, notable differences between the new RPI records and the two reference stacks (Fig. 6), particularly in the 0-30 ka and 60-80 ka intervals, and in the timing of RPI minima at ~115 ka and ~190 ka which correspond to the Blake and Iceland Basin excursions. For ages >250 ka (below ~35 mbsf), the amplitude of RPI proxies is subdued relative to the PISO reference record.

6. Rock magnetism

In addition to data acquired for NRM and RPI investigations, low-field volume susceptibility (κ) was measured at 1-cm intervals using a susceptibility track designed for u-channel samples that has a Gaussian-shaped response function, with width at half height of ~4 cm, similar to the response function of the u-channel magnetometer (Thomas et al., 2003). Following King et al. (1983), the ratio of anhysteretic susceptibility (κ_{ARM}, ARM intensity divided by the DC bias field used to acquire the ARM) to susceptibility (κ) can be used to estimate the "average" or bulk grain size of magnetite. This ratio for cores MD07-3076Q and MD07-3077 has a wide range of values (Fig. 7a). Ratios corresponding to bulk grain sizes <1 µm are from the top 1.3 m in core MD07-3076Q (purple triangles in Fig. 7a).

Additional magnetic mineralogical information was obtained for magnetic hysteresis parameters measured on a Princeton Measurements Corp. vibrating sample magnetometer (VSM). Hysteresis ratios: M_{rs}/M_s and B_{cr}/B_c where M_{rs} is the saturation remanence, M_s is the saturation magnetization, B_{cr} is the coercivity of remanence, and B_c is the coercive force, can be used to delineate single domain (SD), pseudo-single domain (PSD) and multidomain (MD) magnetite and to assign bulk magnetite grain sizes through empirical and theoretical calibrations of the so-called Day plot (Day et al., 1977; Carter-Stiglitz et al., 2001; Dunlop, 2002; Dunlop and Carter-Stiglitz, 2006). The Day-plot for samples from cores MD07-3076Q and MD07-3077, by comparison with measurements of unannealed sized magnetites (Dunlop, 2002), is consistent with the presence of magnetite with bulk grain sizes in the 0.1-3 μm range (Fig. 7b), which is broadly consistent with the κ_{ARM} versus κ plot (Fig. 7a). Note that these "average" (bulk) magnetite grain size estimates are function of grain size mixing over an undetermined grain-size range.

Magnetic hysteresis properties were also analyzed using first-order reversal curves (FORCs) that provide enhanced mineral and domain state discrimination (Pike et al., 1999; Roberts et al., 2000; Muxworthy and Roberts, 2007). FORCs are measured by progressively saturating a small (few hundred mg) sample in a field (B_{sat}), decreasing the field to B_a, reversing the field and sweeping it back to B_{sat} in a series of regular field steps (B_b). The process is repeated for many values of B_a. The magnetization is then represented as a contour plot with axes B_c and B_u where $B_c=(B_b-B_a)/2$ and $B_u=(B_b+B_a)/2$. The contoured FORC distribution can be interpreted in terms of the coercivity distribution along the B_c axis, and spreading of the distribution along the B_u axis provides a measure of magnetostatic interactions for SD grains or internal demagnetizing fields for MD grains. The latter dominates in weakly magnetized deep-sea sediments, and spreading in B_u combined with low B_c can be interpreted in terms of high MD magnetite content. In general, closed peaked structures along the B_c axis are characteristic of SD grains, with contours becoming progressively more parallel to the B_u axis with grain-size coarsening. FORC diagrams were analyzed using the software of Harrison and Feinberg (2008) with a smoothing factor (SF) of 6 for a protocol using an averaging time of 1 s and a field increment of 2 mT up to a maximum applied field of 1 T.

FORC diagrams from the uppermost sediments of core MD07-3076Q, corresponding to high κ_{ARM}/κ values (fine magnetite grain sizes), are characterized by a pronounced ridge along the B_c axis and low dispersion along the B_u axis (Fig. 7c). This pattern implies weak magnetostatic interactions and dispersed fine-grained biogenic magnetite (see examples in Egli et al., 2010; Roberts et al., 2011, 2012; Yamazaki, 2012; Channell et al., 2013). In contrast, FORC diagrams from below ~1.3 mbsf have lower coercivities (B_c) and more divergent FORC distributions along the B_u axis, which is indicative of the increased abundance of coarser magnetite (Fig. 7d).

7. Transmission Electron Microscopy

For transmission electron microscope (TEM) imaging, magnetic extracts were prepared from MD07-3076Q at 0.86-0.91 mbsf (~14 ka) and 2.20-2.25 mbsf (~30 ka). The ~20 cm^3 sediment samples were sonicated in a sodium metaphosphate dispersant. The solutions were loaded into a reservoir that feeds a circulating system driven by a peristaltic pump that allows the fluid to pass slowly, without turbulence, past the outside of a test-tube containing a rare-earth magnet. The material that adhered to the outside of the test-tube was then removed to a methanol solution using a methanol squeeze-bottle. Grains of magnetic separate were adhered to a 3-mm copper TEM grid using another magnet suspended a few cm above the floating grid (see Chang et al., 2012).

Magnetic particles were imaged using a JEOL JEM-2010F high-resolution (HR) TEM in conjunction with energy dispersive x-ray spectroscopy (EDS) at an accelerating voltage of 200 kV. The microscope is equipped with a GatanMultiScan Camera Model 794 for imaging and an Oxford Instruments detector with INCA 4.05 software for microanalysis. Spot analysis and line-scans were conducted in scanning TEM (STEM) mode with a nominal ~1 nm probe size and a camera length of 12 cm.

In the sample from ~0.86-0.91 mbsf (~14 ka), euhedral grains, generally smaller than 100 nm across, but occasionally reaching 200 nm, were observed (Fig. 8 a,b). The shape and size of these grains is consistent with them being magnetosomes produced by magnetotactic bacteria (see Kopp and Kirschvink, 2008; Egli et al., 2010, Roberts et al., 2011, 2012; Yamazaki, 2012). Magnetite octahedra (rectangular shapes with flattened corners) and arrowhead shapes (Fig. 8 a,b) are reminiscent of shapes of bacterial magnetite observed off the SW Iberian Margin (Channell et al., 2013) and elsewhere (Kopp and Kirschvink, 2008). In the sample from 2.20-2.25 mbsf (~30 ka), the magnetite population is apparently different, with rare bacterial magnetite grains but abundant larger irregular-shaped detrital magnetite grains (Fig. 8 c). EDS elemental analyses indicate that the irregular-shaped (detrital) grains contain Fe, O, and Ti, (Fig. 8 b,c) whereas the finer euhedral (biogenic) magnetites contain Fe and O, but no detectable Ti (Fig. 8 b). The lack of Ti in magnetosome magnetite provides a well-documented means (besides grain shape and size) of distinguishing detrital and biogenic magnetite. The predominance of ultra-fine biogenic magnetite in the sample from ~0.86-0.91 mbsf (~14 ka) is consistent with the existence of ultra-fine magnetite in the Holocene of core MD07-3076Q (Fig. 7a, c).

8. Discussion

The ages of onset and cessation of the Laschamp directional excursion at 41.4 ka and 40.4 ka (Fig. 9) are consistent, at centennial scale, with the Laschamp age and duration determined by correlation of the $\delta^{18}O$ record from North Atlantic Ocean core PS2644-5 (Voelker et al., 1998) to the GISP2 ice core (Laj et al., 2000), and with the GICC05 age (41.25 ±0.8 ka) of the center of the ^{10}Be maximum that corresponds to the Laschamp excursion in the GRIP ice core (Yiou et al., 1997; Svensson et al., 2006, 2008). Our South Atlantic result is also consistent with the mid-point age of 41.3 ± 0.6 ka for the Laschamp excursion (Laj et al., 2014) based mainly on $^{40}Ar/^{39}Ar$ age determinations from the Chaines des Puys (France), assuming an Alder Creek

(AC) rhyolite standard age of 1.193 Ma, which is equivalent to 28.02 Ma for the Fish Canyon (FC) sanidine standard advocated by Renne et al. (1998). If more recent estimates for the ages of the AC and FC standards are used (1.2061 Ma and 28.305 Ma; Renne et al., 2010), then the 41.3 ka age for the Laschamp excursion increases to 42.0 ka, which is just outside our estimate based on correlation to the EDC ice core (Fig. 9). This discrepancy may imply issues with the newer standard ages, as observed for the M-B boundary (Channell et al., 2010).

Our Laschamp age estimate is consistent with U-Th dating of a North American speleothem that records of the Laschamp excursion at 41.1 ±0.35 ka (Lascu et al., 2016), although their estimated duration for the directional excursion (2.5 kyr) is 2.5 times greater than estimated here. The Laschamp record from ODP Site 1233 off Chile yields an excursion age centered at 41.0 ka, and a duration for southern hemisphere VGPs of ~600 yr (Stoner et al., 2008), lower than our estimate.

From correlation of MD07-3076Q SST data to the EDC δD record, the onset of the Laschamp excursion coincides with Antarctic Isotopic Maximum (AIM) 10 warm episode (Fig. 9), and hence with Greenland Interstadial (GI) 10 according to inter-hemispheric correlations (Veres et al., 2013). The end of the Laschamp excursion appears to coincide with AIM 9 and Greenland Stadial (GS) 10. In the Antarctic EDC ice core, a broad irregular ^{10}Be flux peak in the 39.5 ka to 42.5 ka interval (AICC2012 age) is accompanied by a distinct nitrate flux peak centered at 41.2 ka (Fig. 9e, Traversi et al., 2016). Nitrate and ^{10}Be fluxes depend partially on the intensity of cosmic ray flux into Earth's upper atmosphere, and are therefore modulated by geomagnetic field intensity. The EDC nitrate peak is apparently closely synchronous with the Laschamp directional excursion recorded in core MD07-3076Q. The EDC ^{10}Be peak is broader than the nitrate peak and generally coincides with the RPI minimum from MD07-3076Q (Figs. 6 and 9e).

The Iceland Basin excursion coincides with the later part of the MIS 6e/7a boundary (terminology of Railsback et al., 2015) in the Antarctic δD record (Fig. 9b,d) which yields a mid-point excursion age of 188.5 ka and duration of ~3.5 kyr. Both age and duration estimates depend on the criteria for defining the excursion. Here we use component magnetization inclination values >-40° to define the directional excursion. For the Iceland Basin excursion recorded in the North Atlantic Ocean, estimated mid-point ages are in the 189-190 ka range (Channell, 2014).

The two RPI proxies (slopes of NRM/ARM and NRM/IRM) are inconsistent in the 0-20 ka interval, which also corresponds to a notable departure from the RPI reference templates (SAPIS and PISO) (Fig. 6). This interval, in turn, corresponds to high concentrations of biogenic magnetite. We conclude that the presence of biogenic magnetite results in over-normalization when using NRM/ARM as the RPI proxy and under-normalization when using NRM/IRM (see Ouyang et al., 2014). In addition, the calibrated RPI templates (e.g. SAPIS and PISO) are poorly defined in the last ~30 kyr, due to their reliance on ODP and MD cores which are characterized by poor core-quality in the uppermost few meters. The fit of MD07-3076Q/3077 RPI proxies to PISO/SAPIS is also poor in the 60-80 ka interval, and RPI minima at ~115 ka and ~190 ka are offset (Fig. 6), possibly implying poor definition of the RPI templates. The large (25 x 25 cm) square-section piston core (MD07-3076Q) is likely to be less affected by stretching artifacts compared to ODP and MD cores.

Below the interval of high biogenic magnetite concentration (0-20 ka), a plausible fit of RPI proxies to the reference templates can be made down to depths corresponding to ~250 ka (Fig.

6). Prior to 250 ka, below ~32 mbsf, RPI proxies are muted relative to the templates, NRM intensities are decreased (Fig. 3), and the MDF of NRM increases. These changes are attributed to progressive magnetite dissolution as a result of microbial sulfate reduction, formation of pore-water sulfide, and reduction of magnetite to form iron sulfides, a process that is ubiquitous in pelagic sediments other than highly oxidized facies such as Pacific red clays. The enhanced reactivity of fine grains results in magnetite grain-size coarsening down-core as dissolution proceeds. The presence of ultra-fine (biogenic) magnetite, from TEM observations (Fig. 8) and rock magnetic data (Fig. 7), imply high concentrations of biogenic magnetite in the uppermost sediments.

9. Conclusions

The Laschamp and Iceland Basin excursions are documented in cores MD07-3076Q and MD07-3077, respectively, by discrete samples and u-channel samples (Fig. 9). Recording of the Laschamp and Iceland Basin excursions is facilitated by sedimentation rates of ~20 cm/kyr and ~10 cm/kyr in the two excursion intervals, respectively (Fig. 2a). The millennial-scale duration of the Laschamp and Iceland Basin directional excursions (~1 kyr and ~3.5 kyr, respectively) results in rare recordings of excursions in sedimentary sequences with normal pelagic sedimentation rates (<10 cm/kyr). Sedimentary records of magnetic excursions are often compromised by bioturbation and non-instantaneous magnetic remanence acquisition, the inherent brevity of magnetic excursions, and by down-core magnetite dissolution that preferentially affects fine-grained biogenic magnetite.

The documentation and timing of the Laschamp and Iceland Basin excursions in the South Atlantic Ocean augments the few other recordings of these excursions in the southern hemisphere (cited above). The age models for cores MD07-3076Q and MD07-3077 were built through radiocarbon and sea-surface temperature proxies tied to Antarctic ice core records, and are supported by the resulting coincidence of the marine Laschamp excursion record with cosmogenic ^{10}Be and nitrate fluxes in the EDC Antarctic ice core (Fig. 9). Excursion mid-point ages and durations determined from the age models are 40.9 ka and ~1 kyr for the Laschamp excursion, and 188 ka and ~3.5 kyr for the Iceland Basin excursion, respectively, using inclination values >-40° to define the stratigraphic intervals over which the excursions are recorded (Fig. 9). We observe no discrepancies in the ages of the Laschamp or Iceland Basin excursions between the North and South Atlantic Oceans as has been mooted for both the M-B reversal and the Laschamp excursion (Leonhardt and Fabian, 2007; Leonhardt et al., 2009).

Acknowledgements

We thank Kainian Huang for laboratory assistance, and Andrew Roberts for a thorough review of the manuscript. This research was supported by US National Science Foundation grants OCE-0850413 and EAR-1014506 (to JC), NERC grant NE/J010545/1 (to LCS), Gates Cambridge Scholarship (to JG), and AXA Research Fund Post-doctoral Fellowship (to NVR). CW acknowledges support from European Research Council grant ACCLIMATE/no 339108. This is LSCE contribution 5666.

References

Banerjee, S.K., Mellema, J.P., 1974. A new method for the determination of paleointensity from the ARM properties of rocks. Earth Planet. Sci. Lett., 23, 177-184.

Bazin, L., Landais, A., Lemieux-Dudon, B., Toyé Mahamadou Kele, H., Veres, D., Parrenin, F., Martinerie, P., Ritz, C., Capron, E., Lipenkov, V., Loutre, M.F., Raynaud, D., Vinther, B.M., Svensson, A., Rasmussen, S.O., Severi, M., Blunier, T., Leuenberger, M., Fischer, H., Masson-Delmotte, V., Chappellaz, J., Wolff, E., 2013. An optimized multi-proxy, multi-site Antarctic ice and gas orbital chronology (AICC2012): 120 - 800 ka. Clim. Past 9, 1715-1731.

Blunier, T., Brook, E., 2001. Timing of millennial-scale climate change in Antarctica and Greenland during the last glacial period. Science, 291, 109-112.

Carter-Stiglitz, B., Moskowitz, B., Jackson, M., 2001. Unmixing magnetic assemblages and the magnetic behavior of bimodal mixtures. J. Geophys. Res., 106, 26,397-26, 411.

Chang, L., Roberts, A.P., Williams, D., Fitz Gerald, J.D., Larrasoana, J.C., Jovane L., Muxworthy, A.R., 2012. Giant magnetofossils and hyperthermal events. Earth Planet. Sci. Letters, 351-352, 258-269.

Channell, J.E.T., 1999. Geomagnetic paleointensity and directional secular variation at Ocean Drilling Program (ODP) Site 984 (Bjorn Drift) since 500 ka: comparisons with ODP Site 983 (Gardar Drift). J. Geophys. Res., 104, 22,937-22,951.

Channell, J.E.T., 2006. Late Brunhes polarity excursions (Mono Lake, Laschamp, Iceland Basin and Pringle Falls) recorded at ODP Site 919 (Irminger Basin). Earth Planet. Sci. Lett., 244, 378-393.

Channell, J.E.T., 2014. The Iceland Basin excursion: age, duration, and excursion field geometry. Geochem. Geophys. Geosyst., 15, 4920-4935, doi:10.1002/2014GC005564.

Channell, J.E.T., Hodell D.A., Lehman, B., 1997. Relative geomagnetic paleointensity and $\delta^{18}O$ at ODP Site 983 (Gardar Drift, North Atlantic) since 350 ka. Earth Planet. Sci. Lett., 153, 103-118.

Channell, J.E.T., Stoner, J.S., Hodell, D.A., Charles, C.D., 2000. Geomagnetic paleointensity for the last 100 kyr from the sub-antarctic South Atlantic: a tool for inter-hemispheric correlation. Earth Planet. Sci. Lett., 175, 145-160.

Channell, J.E.T., Mazaud, A., Sullivan, P., Turner, S., and Raymo, M.E., 2002. Geomagnetic excursions and paleointensities in the Matuyama Chron at Ocean Drilling Program Sites 983 and 984 (Iceland Basin). J. Geophys. Res., 107, 2114, doi:10.1029/2001JB000491.

Channell, J.E.T., Xuan, C. and Hodell, D.A., 2009. Stacking paleointensity and oxygen isotope data for the last 1.5 Myrs (PISO-1500). Earth Planet. Sci. Lett., 283, 14-23.

Channell, J.E.T., Hodell, D.A., Singer, B.S., Xuan, C., 2010. Reconciling astrochronological and $^{40}Ar/^{39}Ar$ ages for the Matuyama-Brunhes boundary and late Matuyama Chron. Geochem. Geophys. Geosyst., 11, Q0AA12, doi:10.1029/2010GC003203.

Channell, J.E.T., Hodell, D.A., Curtis, J.H., 2012. ODP Site 1063 (Bermuda Rise) revisited: oxygen isotopes, excursions and paleointensity in the Brunhes Chron. Geochem. Geophys. Geosyst., 13, Q02001, doi:10.1029/2011GC003897.

Channell, J.E.T., Hodell, D.A., Margari, V., Skinner, L.C., Tzedakis, P.C., Kesler, M.S., 2013. Biogenic magnetite, detrital hematite, and relative paleointensity in sediments from the Southwest Iberian Margin, Earth Planet. Sci. Lett., 376, 99-109.

Charles, C.D., Lynch-Stieglitz, J., Ninnemann, U.S., Fairbanks R.G., 1996. Climate connections between the hemispheres revealed by deep sea sediment core/ice core correlations. Earth Planet. Sci. Lett,, 142, 19-27.

Collins, L.G., Hounslow, M.W., Allen, C.S., Hodgson, D.A., Pike, J., Karloukovski, V.V., 2012. Palaeomagnetic and biostratigraphic dating of marine sediments from the Scotia Sea, Antarctica: First identification of the Laschamp excursion in the Southern Ocean. Quart. Geochron., 7, 67-75.

Day, R., Fuller, M., Schmidt, V.A., 1977. Hysteresis properties of titanomagnetites: grain-size and compositional dependence. Phys. Earth Planet. Inter., 13, 260-267.

Dunlop, D.J., 2002. Theory and application of the Day plot (M_{rs}/M_s versus H_{cr}/H_c) 1. Theoretical curves and tests using titanomagnetite data. J. Geophys. Res., 107, B3, 2056, doi:10.1029/2001JB000486.

Dunlop, D.J., Carter-Stiglitz, B., Day plots of mixtures of superparamagnetic, single domain, pseudosingle domain, and multidomain magnetites. J. Geophys. Res., 111, B12S09, doi: 10.1029/2006JB004499.

Egli, R., Chen, A.P., Winklhofer, M., Kodama K.P., Horng, C-S., 2010. Detection of non-interacting single domain particles using first-order reversal curve diagrams. Geochem. Geophys. Geosyst., 11, Q01Z11, doi:10.1029/2009GC002916.

Evans, H.F., Channell, J.E.T., Stoner, J.S., Hillaire-Marcel, C, Wright, J.D., Neitzke, L.C., Mountain, G.S., 2007. Paleointensity-assisted chronostratigraphy of detrital layers on the Eirik Drift (North Atlantic) since marine isotope stage 11. Geochem. Geophys. Geosyst., 8, Q11007, doi: 10.1029/2007GC001720.

Gottschalk, J., Skinner, L.C., Waelbroeck, C., 2015a. Contribution of seasonal sub-Antarctic surface water variability to millennial-scale changes in atmospheric CO_2 over the last deglaciation and Marine Isotope Stage 3. Earth Planet. Sci. Letters, 411, 87-99.

Gottschalk, J., Skinner, L.C., Misra, S., Waelbroeck, C., Menviel, L., Timmermann, A., 2015b. Abrupt changes in the southern extent of North Atlantic Deep Water during Dansgaard-Oeschger events, Nature Geosci., 8, 950-955.

Guyodo, Y., Channell, J.E.T., Thomas, R., 2002. Deconvolution of u-channel paleomagnetic data near geomagnetic reversals and short events. Geophys. Res. Letters, 29, 1845, doi:10.1029/2002GL014963.

Harrison, R.J., Feinberg, J.M., 2008. FORCinel: an improved algorithm for calculating first-order reversal curve distributions using locally weighted regression smoothing. Geochem., Geophys., Geosyst., 9, Q05016, doi:10.1029/2008GC001987.

Hodell, D. A., Charles, C.D., Sierro, F., 2001. Late Pleistocene evolution of the ocean'scarbonate system, Earth Planet. Sci. Lett., 192, 109–124.

Jouzel, J., Masson-Delmotte, V., Cattani, O., Dreyfus, G., Falourd, S., Hoffmann, G., Minster, B., Nouet, J., Barnola, J.M., Chappellaz, J., Fischer, H., Gallet, J.C., Johnsen, S., Leuenberger, M., Loulergue, L., Luethi, D., Oerter, H., Parrenin, F., Raisbeck, G., Raynaud, D., Schilt, A., Schwander, J., Selmo, E., Souchez, R., Spahni, R., Stauffer, B., Steffensen, J.P., Stenni, B., Stocker, T.F., Tison, J.L., Werner, M., Wolff, E.W., 2007. Orbital and millennial Antarctic climate variability over the past 800,000 years. Science, 317, 793-796.

King, J.W., Banerjee, S.K., Marvin, J., 1983. A new rock-magnetic approach to selecting sediments for geomagnetic paleointensity studies: application to paleointensity for the last 4000 years. J. Geophys. Res. 88, 5911-5921.

Kirschvink, J.L., 1980. The least squares lines and plane analysis of paleomagnetic data. Geophys. J.R. Astron. Soc. 62, 699-718.

Kopp, R.E., Kirschvink, J.L., 2008. The identification and biogeochemical interpretation of fossil magnetotactic bacteria. Earth Sci. Rev., 86, 42-61.

Laj, C., Kissel, C., Mazaud, A., Channell, J.E.T., Beer, J., 2000. North Atlantic paleointensity stack since 75 ka (NAPIS-75) and the duration of the Laschamp event. Phil. Trans. R. Soc. Lond., 358, 1009-1025.

Laj, C., Kissel, C., Roberts, A.P., 2006. Geomagnetic field behavior during the Icelandic Basin and Laschamp geomagnetic excursions: a simple transitional field geometry? Geochem. Geophys. Geosyst., 7, Q03004, doi :10,1029/2005GC001122.

Laj, C., Guillou, H., Kissel, C., 2014. Dynamics of the Earth's magnetic field in the 10-75 kyr period comprising the Laschamp and Mono Lake excursions: new results from the French Chaine des Puys in a global perspective. Earth Planet. Sci. Lett., 387, 184-197.

Lamy, F., Kaiser, J., Ninnemann, U., Hebbeln, D., Arz H.W., Stoner, J., 2004. Antarctic timing of surface water changes off Chile and Patagonian Ice Sheet response. Science, 304, 1959-1962.

Lascu, I., Feinberg, J.M., Dorale, J.A., Cheng, H., Edwards, R.L., 2016. Age of the Laschamp excursion determined by U-Th dating of a speolthem record from North America. Geology, 44, 139-142, doi:10.1130/G37490.1.

Leonhardt, R., Fabian, K., 2007. Paleomagnetic reconstructon of the global geomagnetic field evolution during the Matuyama/Brunhes transition: iterative Bayesian inversion and independent verification. Earth Planet. Sci. Lett., 253, 172-195.

Leonhardt, R., Fabian, K., Winklhofer, M., Ferk, A., Laj C., Kissel, C., 2009. Geomagnetic field evolution during the Laschamp excursion. Earth Planet. Sci. Lett., 278, 87-95.

Levi, S., Banerjee, S.K., 1976. On the possibility of obtaining relative paleointensities from lake sediments. Earth Planet. Sci. Lett., 29, 219-226.

Lund, S.P., Schwartz, M., Keigwin, L., Johnson, T., 2005. Deep-sea sediment records of the Laschamp geomagnetic field excursion (<41,000 calendar years before present). J. Geophys. Res., 110, Q12006, doi :10,1029, 2005GC001036.

Lund, S., Stoner, J.S., Channell, J.E.T., Acton, G., 2006a. A summary of Brunhes paleomagnetic field variability recorded in Ocean Drilling Program cores. Phys. Earth Planet. Inter., 156, 194-204.

Lund, S.P., Stoner, J.S., Lamy, F., 2006b. Late Quarternary paleomagnetic secular variation and chronostratigraphy from ODP Sites 1233 and 1234. In: Tiedemann, R., Mix, A.C., Richter, C., and Ruddiman, W.F. (Eds.), Proc. ODP Sci. Results, 202: College Station , TX (Ocean Drilling Program), 1–22. doi:10.2973/odp.proc.sr.202.208.2006.

Mazaud, A., Sicre, M.A., Ezat, U., Pichon, J.J., Duprat, J., Laj, C., Kissel, C., Beaufort, L., Michel, E., Turon, J.L., 2002. Geomagnetic-assisted stratigraphy and sea surface temperature changes in core MD94-103 (Southern Indian Ocean): possible implications for North-South climatic relationships around H4. Earth Planet. Sci. Lett., 201, 159-170.

Mortyn, P.G., Charles, C.D., Ninnemann, U.S., Ludwig K., Hodell, D.A., 2003. Deep sea sedimentary analogs for the Vostok ice core. Geochem., Geophys., Geosyst., 4, 8405, doi:10.1029/2002GC000475.

Muxworthy, A.R., Roberts, A.P, 2007. First-order reversal curve (FORC) diagrams. In Encyclopedia of Geomagnetism and Paleomagnetism. Gubbins, D. and E. Herrero-Bervera (eds.), 266-272, Springer, Dordrecht, Netherlands.

Nowaczyk, N.R., Frank, U., Kind, J., Arz, H.W., 2013. A high-resolution paleointensity stack of the past 14 to 68 ka from Black Sea sediments. Earth Planet. Sci. Lett., 384, 1-16, 2013.

Oda, H., Nakamura, K., Ikehara, K., Nakano, T., Nishimura, M., Khlystov, O., 2002. Paleomagnetic record from Academician Ridge, Lake Baikal: a reversal excursion at the base of marine oxygen isotope stage 6. Earth Planet. Sci. Lett., 202, 117-132.

Ouyang, T., Heslop, D., Roberts, A.P., Tian, C., Zhu, Z., Qiu, Y., Peng, X., 2014. Variable remanence acquisition efficiency in sediments containing biogenic and detrital magnetites: implications for relative paleointensity signal recording. Geochem. Geophys. Geosyst., 15, 2780-2796, doi:10.1002/2014GC005301.

Pike, C.R., Roberts A.P., Verosub, K.L., 1999. Characterizing interactions in fine magnetic particle systems using first order reversal curves. J. Appl. Phys., 85, 6660-6667.

Railsback, L.B., Gibbard, P.L., Head, M.J., Voarintsoa N.G.R., Toucanne, S., 2015. An optimized scheme of lettered marine isotope substages for the last 1.0 million years, and the climatostratigraphic nature of isotope stages and substages. Quat. Sci. Rev., 111, 94-106.

Renne, P.R.,Swisher, C.C., Deino, A.L., Karner, D.B., Owens, T.L., DePaolo, D.J., 1998. Intercalibration of standards, absolute ages and uncertainties in $^{40}Ar/^{39}Ar$ dating. Chem. Geol., 145, 117-152.

Renne, P.R., Mundil, R., Balco, G., Min K., Ludwig, K.R., 2010. Joint determination of ^{40}K decay constants and $^{40}Ar^{*}/^{40}K$ for the Fish Canyon sanidine standard, and improved accuracy for $^{40}Ar/^{39}Ar$ geochronology. Geochim. Cosmochim. Acta, 74, 5349-5367.

Roberts, A.P., Lehman, B., Weeks, R.J., Verosub K.L., Laj, C., 1997. Relative paleointensity of the geomagnetic field over the last 200,000 years from ODP Sites 883 and 884, North Pacific Ocean. Earth Planet. Sci. Lett., 152, 11-23.

Roberts, A.P., Pike, C.R., Verosub, K.L., 2000. First-order reversal curve diagrams: a new tool for characterizing the magnetic properties of natural samples. J. Geophys. Res., 105, 28,461-28,475.

Roberts, A.P., Florindo, F., Villa, G., Chang, L., Jovane, L., Bohaty, S.M., Larrasoana, J.C., Heslop, D., Fitz Gerald, J.D., 2011. Magnetotactic bacterial abundance in pelagic marine environments is limited by organic carbon flux and availability of dissolved iron. Earth Planet. Sci. Lett., 310, 441-452.

Roberts, A.P., Chang, L., Heslop, D., Florindo, F., Larrasoana, J.C., 2012. Searching for single domain magnetite in the "pseudo-single-domain" sedimentary haystack: implications of biogenic magnetite preservation for sediment magnetism and relative paleointensity determinations. J. Geophys. Res., 117, B08104, doi:10.1029/2012JB009412.

Skinner, L.C., McCave, I.N., 2003. Analysis and modeling of gravity- and piston coring based on soil mechanics. Mar. Geol., 199, 181-209.

Skinner, L.C., Fallon, S., Waelbroeck, C., Michel E., Barker, S., 2010. Ventilation of the Deep Southern Ocean and deglacial CO_2 rise. Science, 328, 1147-1151.

Stoner, J.S., Laj, C., Channell, J.E.T., Kissel, C., 2002. South Atlantic (SAPIS) and North Atlantic (NAPIS) geomagnetic paleointensity stacks (0-80 ka): implications for inter-hemispheric correlation. Quat. Sci. Rev., 21, 1141-1151.

Stoner, J.S., Channell, J.E.T., Hodell, D.A., Charles, C., 2003. A 580 kyr paleomagnetic record from the sub-Antarctic South Atlantic (ODP Site 1089). J. Geophys. Res., 108, 2244, doi:10.1029/2001JB001390.

Stoner, J.S., Lund, S., Channell, J.E.T., Mix, A.C., Davies, M.H., Lamy, F., 2008. High sedimentation rate paleomagnetic records for the last 70 kyrs from the Chilean Margin (ODP

Sites 1233, 1234, 1235). American Geophysical Union, Fall Meeting, Abstract GP14A-02, San Francisco.

Svensson, A., Andersen, K.K., Bigler, M., Clausen, H.B., Dahl-Jensen, D., Davies, S.M., Johnsen, S.J., Muscheler, R., Rasmussen, S.O., Rothlisberger, R., Steffensen, J.P., Vinther, B.M., 2006. The Greenland Ice Core Chronology 2005, 15-42 ka. Part 2: comparison to other records. Quat. Sci. Rev., 25, 3258-3267.

Svensson, A., Andersen, K.K., Bigler, M., Clausen, H.B., Dahl-Jensen, D., Davies, S.M., Johnsen, S.J., Muscheler, R., Parrenin, F., Rasmussen, S.O., Rothlisberger, R., Seierstad, I., Steffensen, J.P., Vinther, B.M., 2008. A 60,000 year Greenland stratigraphic ice core chronology. Clim. Past, 4, 47-57.

Szérémèta, N., Bassinot, F., Balut, Y., Labeyrie, L., Pagel, M., 2004. Oversampling of sedimentary series collected by giant piston corer: evidence and corrections based on 3.5-kHz chirp profiles. Paleoceanography, 19, PA1005, doi:10.1029/2002PA000795.

Tauxe, L., 1993. Sedimentary records of relative paleointensity of the geomagnetic field: theory and practice. Rev. Geophys., 31, 319-354.

Thomas, R., Guyodo, Y., Channell, J.E.T., 2003. U-channel track for susceptibility measurements. Geochem., Geophys. Geosyst., 1050, doi:10.1029/2002GC000454.

Traversi, R., Becagli, S., Poluianov, S., Severi, M., Solanki, S.K., Usoskin I.G., Udisti, R., 2016. The Laschamp geomagnetic excursion featured in nitrate record from EPICA-Dome C ice core. Sci. Rep., 6, 20235; doi: 10-1038/srep20235.

Vázquez Riveiros, N., Waelbroeck, C., Skinner, L., Roche, D.M., Duplessy J-C., Michel, E., 2010. Response of South Atlantic deep waters to deglacial warming during Termination V and I. Earth Planet. Sci. Letters, 298, 323-333.

Vázquez Riveiros, N., Waelbroeck, C., Skinner, L., Duplessy, J-C., McManus, J.F., Kandiano, K.S., Bauch, H.A., 2013. The “MIS 11 paradox” and ocean circulation: role of millennial scale events. Earth Planet. Sci. Lett., 371-372, 258-268.

Veres, D., Bazin, L., Landais, A., Kele, H.T.M., Lemieux-Dudon, B., Parrenin, F., Martinerie, P., Blayo, E., Blunier, T., Capron, E., Chappellaz, J., Rasmussen, S.O., Severi, M., Svensson, A., Vinther, B.M., Wolff, E., 2013. The Antarctic ice core chronology (AICC2012): an optimized multi-parameter and multi-site dating approach for the last 120 thousand years. Clim. Past 9, 1733-1748.

Voelker, A., Sarnthein, M. Grootes, P.M., Erlenkeuser, H., Laj, C., Mazaud, A., Nadeau, M.J., Schleicher, M., 1998. Correlation of marine ^{14}C ages from the Nordic sea with GISP2 isotope record: implication for ^{14}C calibration beyond 25 ka BP. Radiocarbon, 40, 517-534.

Weeks, R., Laj, C., Endignoux, L., Fuller, M., Roberts, A., Manganne, R., Blanchard, E., Goree, W., 1993. Improvements in long-core measurement techniques: applications in palaeomagnetism and palaeoceanography. Geophys. J. Int., 114, 651-662.

Xuan, C., Channell, J.E.T., 2009. UPmag: MATLAB software for viewing and processing u-channel or other pass-through paleomagnetic data. Geochem. Geophys. Geosyst., 10, Q10Y07, doi:1029/2009GC002584.

Yamazaki, T., 2012. Paleoposition of the intertropical convergence zone in the eastern Pacific inferred from glacial-interglacial changes in terregenous and biogenic magnetic mineral fractions. Geology, 40, 151-154.

Yamazaki, T., Ioka, N., 1994. Long-term secular variation of the geomagnetic field during the last 200 kyr recorded in sediment cores from the western equatorial Pacific, Earth Planet. Sci. Lett., 128, 527-544.

Yiou, F., Raisbeck, G.M., Baumgartner, S., Beer, J., Hammer, C., Johnsen, S., Jouzel, J., Kubik, P.W., Lestringuez, J., Stiévenard, M., Suter, M., Yiou, P., 1997. Beryllium 10 in Greenland Ice Core Project ice core at Summit, Greenland. J. Geophys. Res., 102, 26783-26794.

Figure captions

Fig. 1. Map with locations of cores MD07-3076Q and MD07-3077, and ODP Site 1089 (from GeoMapApp™).

Fig. 2. Age models for the studied sediment cores. (a) Inferred sedimentation rates for core MD07-3076Q (red) and MD07-3077 (blue) with age tie-points (blue/red points) listed in Tables 1 and 2. (b) δD from the EPICA Dome C (EDC) ice core (Jouzel et al., 2007) placed on the AICC2012 chronology (Bazin et al., 2013; Veres et al., 2013). (c) Percentage of *G. bulloides* for cores MD07-3076Q (red) and MD07-3077 (blue). (d) Percentage *N. pachyderma* (sin.) for cores MD07-3076Q (red) and MD07-3077 (blue). (e) Blue reflectance for cores MD07-3076Q (red) and MD07-3077 (blue). At base: expanded versions of (b), (c) and (d) for core MD07-3076Q in the 24-68 ka interval (left), and for core MD07-3077 in the 145-194 ka interval (right). For percentages of *G. bulloides* and *N. pachyderma*, the data points, smoothed lines, and standard deviations are shown.

Fig. 3. Component magnetization directions with stratigraphic position of the Laschamp and Iceland basin excursions in cores MD07-3076Q (red) and MD07-3077 (blue). Component declination, inclination and maximum angular deviation (MAD) values computed for the 20-80 mT demagnetization interval from u-channel samples plotted versus depth (meters below seafloor, mbsf). Natural remanent magnetization (NRM) intensities after 20 mT peak AF demagnetization decrease below ~32 mbsf, attributed to diagenetic magnetite dissolution.

Fig. 4. U-channel and discrete sample paleomagnetic data for the Laschamp excursion (left: core MD07-3076Q) and Iceland Basin excursion (right: core MD07-3077) versus depth (meters

below seafloor, mbsf). Component inclinations (red symbols with line for u-channel data, orange triangles for discrete samples), component declinations (blue circles for u-channel data, light blue triangles for discrete samples) and maximum angular deviation (MAD) values for u-channels (green dots) and discrete samples (black triangles). Shaded intervals indicate intervals yielding clearly excursional magnetization directions, defined here by inclination values >-40°.

Fig. 5. Orthogonal projections of alternating field demagnetization data for (a) discrete samples in the vicinity of the Laschamp excursion (core MD07-3076Q), (b) discrete samples in the vicinity of the Iceland Basin excursion (core MD07-3077), (c) u-channel samples that record the Laschamp excursion in core MD07-3076Q and the Iceland Basin excursion in core MD07-3077. Red lines/symbols represent projections onto the vertical plane. Blue lines/symbols represent projections onto horizontal plane. Depths in the cores and ages associated with each orthogonal projection are indicated. Natural remanent magnetization (NRM) measurements prior to demagnetization were followed by demagnetization at peak fields of 10-50 mT in 2.5 mT steps, and between 50 and 90 mT in 5 mT steps. All projections have West and Up towards top of page. Magnetization intensities x10^{-2} A/m.

Fig. 6. PISO relative paleointensity (RPI) stack (black) (Channell et al., 2009) with SAPIS RPI stack (green) (Stoner et al., 2002). Core MD07-3076Q and MD07-3077 RPI proxies: NRM/ARM (light blue/blue) and NRM/$IRM_{0.3T}$ (orange/red) placed on the adopted age model.

Fig. 7. (a) Plot of anhysteretic susceptibility (κ_{ARM}) versus susceptibility (κ) for core MD07-3076Q (blue dots, purple triangles are from the Holocene interval) and MD07-3077 (red dots) with calibration of magnetite grain size from King et al. (1983). (b) Hysteresis ratio plot after Day et al. (1977) for samples from core MD07-3076Q (black squares) and core MD07-3077 (red

circles), which lie along a magnetite grain-size mixing line (blue triangles) in the pseudo-single domain (PSD) field, between the single domain (SD) and multidomain (MD) fields. Green squares: hysteresis ratios from crushed, sized (unannealed) natural titanomagnetite (Dunlop, 2002). (c) First-order reversal curve (FORC) diagram for Holocene sediments at 0.5 mbsf in core MD07-3076Q (10.07 ka). (d) FORC diagram from the last glacial maximum at 1.31 m in core MD07-3076Q (18.84 ka). FORC diagrams were processed using a smoothing factor of 6.

Fig. 8. Transmission electron microscope (TEM) images of magnetic mineral extracts. (a) Typical biogenic magnetite grains from a depth of 0.86-0.90 mbsf in core MD07-3076Q. (b) Typical biogenic magnetite grains with a detrital magnetite grain at the top right from the same magnetic extract (0.86-0.90 mbsf) with position (red line) of an energy dispersive x-ray spectroscopy (EDS) line scan, with counts from the line scan (right). Presence or absence of Ti indicates detrital or biogenic magnetite, respectively. (c) Detrital magnetite grain from a depth of 2.20-2.30 mbsf in core MD0-3076Q with the position (red dot) of EDS analysis (right). White bars provide scales for each micrograph.

Fig. 9. Laschamp (left) and Iceland Basin excursion (right) in cores MD07-3076Q and MD07-3077, respectively, versus age (ka). (a and b) Percentage of *N. pachyderma* (sin.) (blue) and *G. bulloides* (red) compared with δD (black) from the EPICA (EDC) ice core (Jouzel et al., 2007) placed on the AICC2012 chronology (Bazin et al., 2013; Veres et al., 2013). Antarctic Isotopic Maxima (AIM 8-11, EPICA Community members, 2006) and Greenland Stadials (GS) and Interstadials (GI) correlated after Veres et al. (2013). (c and d) Component inclinations (red dots with line for u-channel data, orange triangles for discrete samples), component declinations (blue circles for u-channel data, light blue triangles for discrete samples) plotted versus age.

Component declinations/inclinations computed for a uniform 20-80 mT peak AF demagnetization interval for both u-channel and discrete sample data. Shaded intervals demarcate clear excursional directions, defined here by inclination values >-40°. (e) EPICA cosmogenic fluxes for 38.5-44.0 ka (Traversi et al., 2016) for ^{10}Be (orange) with a 10 point running mean (red), and nitrate (light green) with a 10 point running mean (dark green), compared with RPI proxies from core MD07-3076Q (from Fig. 6 with NRM/ARM slope in dark blue and NRM/IRM slope in light blue).

Table 1. Age model for Core MD07-3076Q

Depth (cm)	Age (ka)	Ref./Basis	Depth (cm)	Age (ka)	Ref./Basis
1.5000	1.2030	1/radiocarb.	113.50	17.113	1/radiocarb.
5.5000	1.6250	1/radiocarb.	117.50	17.578	1/radiocarb.
9.5000	2.2400	1/radiocarb.	119.50	17.802	1/radiocarb.
15.500	3.2970	1/radiocarb.	121.50	18.006	1/radiocarb.
21.500	4.7340	1/radiocarb.	125.50	18.381	1/radiocarb.
25.500	5.6580	1/radiocarb.	133.50	19.042	1/radiocarb.
31.500	6.5430	1/radiocarb.	137.50	19.403	1/radiocarb.
35.500	7.0180	1/radiocarb.	145.50	20.512	1/radiocarb.
41.500	8.4550	1/radiocarb.	161.50	22.881	1/radiocarb.
45.500	9.3530	1/radiocarb.	173.50	24.743	1/radiocarb.
49.500	10.003	1/radiocarb.	187.50	26.234	1/radiocarb.
53.500	10.569	1/radiocarb.	197.50	27.380	1/radiocarb.
55.500	10.847	1/radiocarb.	237.00	30.062	% *G. bulloides*
59.500	11.277	1/radiocarb.	290.60	33.655	% *G. bulloides*
61.500	11.538	1/radiocarb.	325.60	35.848	% *G. bulloides*
63.500	11.842	1/radiocarb.	368.40	38.264	% *G. bulloides*
67.500	12.536	1/radiocarb.	427.30	41.264	% *G. bulloides*
73.500	13.043	1/radiocarb.	459.80	43.092	% *G. bulloides*
77.500	13.405	1/radiocarb.	491.60	45.928	% *G. bulloides*
85.500	14.362	1/radiocarb.	595.90	53.903	% *G. bulloides*
89.500	14.670	1/radiocarb.	687.30	59.576	% *G. bulloides*
91.500	14.792	1/radiocarb.	760.40	66.111	% *G. bulloides*
95.500	14.938	1/radiocarb.	906.70	84.941	Refl./3077
99.500	15.205	1/radiocarb.	991.70	95.571	Refl./3077
109.50	16.590	1/radiocarb.	1089.8	107.08	Refl./3077

Ref 1: Skinner et al. (2010)

Table 2. Age model for Core MD07-3077

Depth (cm)	Corrected depth (cm)	Age (ka) AICC2012	Basis
0.0000	0.0000	1.0450	Refl. from MD07-3076Q
197.10	197.10	18.682	Refl. from MD07-3076Q
292.00	292.00	27.323	Refl. from MD07-3076Q
647.20	647.20	36.492	Refl. from MD07-3076Q
768.00	768.00	39.975	Refl. from MD07-3076Q
901.20	901.20	43.850	Refl. from MD07-3076Q
1023.2	1023.2	48.428	Refl. from MD07-3076Q
1397.0	1397.0	64.806	Refl. from MD07-3076Q
1578.1	1578.1	77.122	Planktic $\delta^{18}O$
1700.1	1700.1	88.143	Planktic $\delta^{18}O$
1932.0	1932.0	108.39	% *N. pachyderma* (sin.)
2030.6	1989.6	119.57	% *N. pachyderma* (sin.)
2068.5	2027.5	126.03	% *N. pachyderma* (sin.)
2136.3	2095.3	131.80	% *N. pachyderma* (sin.)
2164.9	2123.9	136.15	% *N. pachyderma* (sin.)
2305.8	2264.8	150.58	% *N. pachyderma* (sin.)
2345.2	2304.2	154.51	% *G. bulloides*
2379.6	2338.6	156.78	% *G. bulloides*
2399.8	2358.8	160.26	% *G. bulloides*
2441.8	2400.8	163.67	% *G. bulloides*
2490.3	2449.3	170.25	% *G. bulloides*
2541.3	2500.3	174.63	% *G. bulloides*
2561.5	2520.5	178.19	% *G. bulloides*
2590.3	2549.3	180.87	% *G. bulloides*
2682.3	2641.3	190.12	% *G. bulloides*
2730.0	2689.0	195.26	% *N. pachyderma* (sin.)
2777.0	2736.0	201.88	% *N. pachyderma* (sin.)
2805.3	2764.3	205.10	% *N. pachyderma* (sin.)
2887.8	2846.8	217.11	% *N. pachyderma* (sin.)
2915.7	2874.7	224.62	% *N. pachyderma* (sin.)
2939.9	2898.9	227.66	% *N. pachyderma* (sin.)
2948.2	2907.2	229.89	% *N. pachyderma* (sin.)
3000.1	2959.1	237.27	% *N. pachyderma* (sin.)
3039.5	2998.5	243.07	% *N. pachyderma* (sin.)
3101.5	3060.5	247.81	% *N. pachyderma* (sin.)

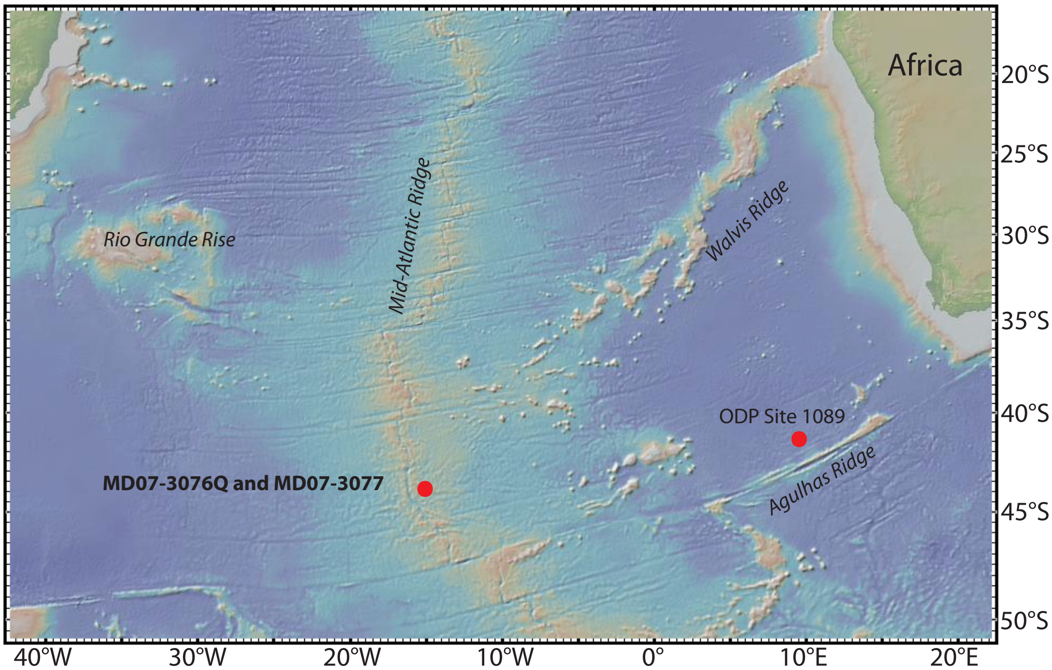
Africa
Rio Grande Rise
Mid-Atlantic Ridge
Walvis Ridge
ODP Site 1089
Agulhas Ridge
MD07-3076Q and MD07-3077
20°S
25°S
30°S
35°S
40°S
45°S
50°S
40°W
30°W
20°W
10°W
0°
10°E
20°E

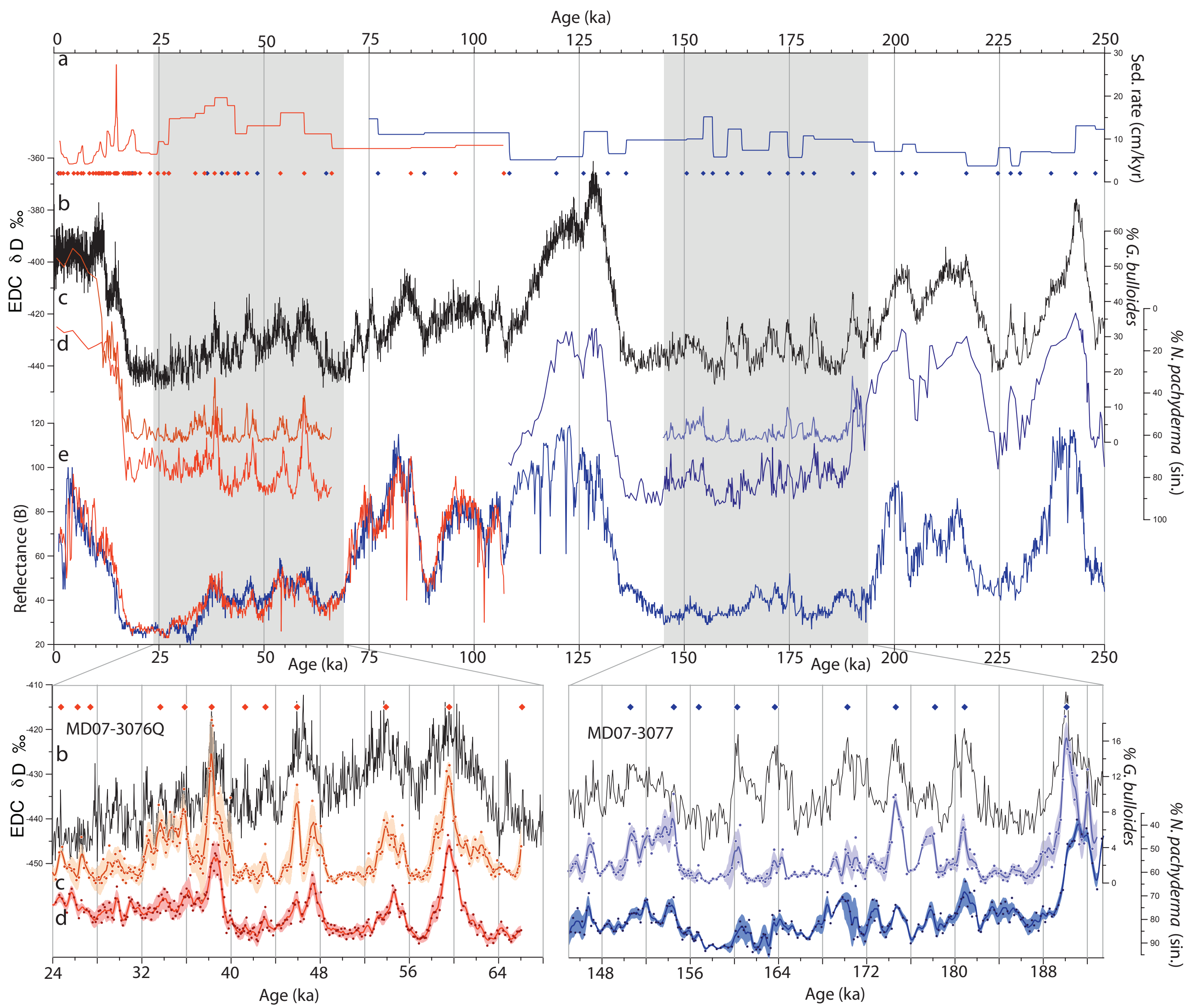

Age (ka)
a
b
c
d
e
EDC δD ‰
Reflectance (B)
Sed. rate (cm/kyr)
% G. bulloides
% N. pachyderma (sin.)
Age (ka)
Age (ka)
MD07-3076Q
MD07-3077
Age (ka)
Age (ka)

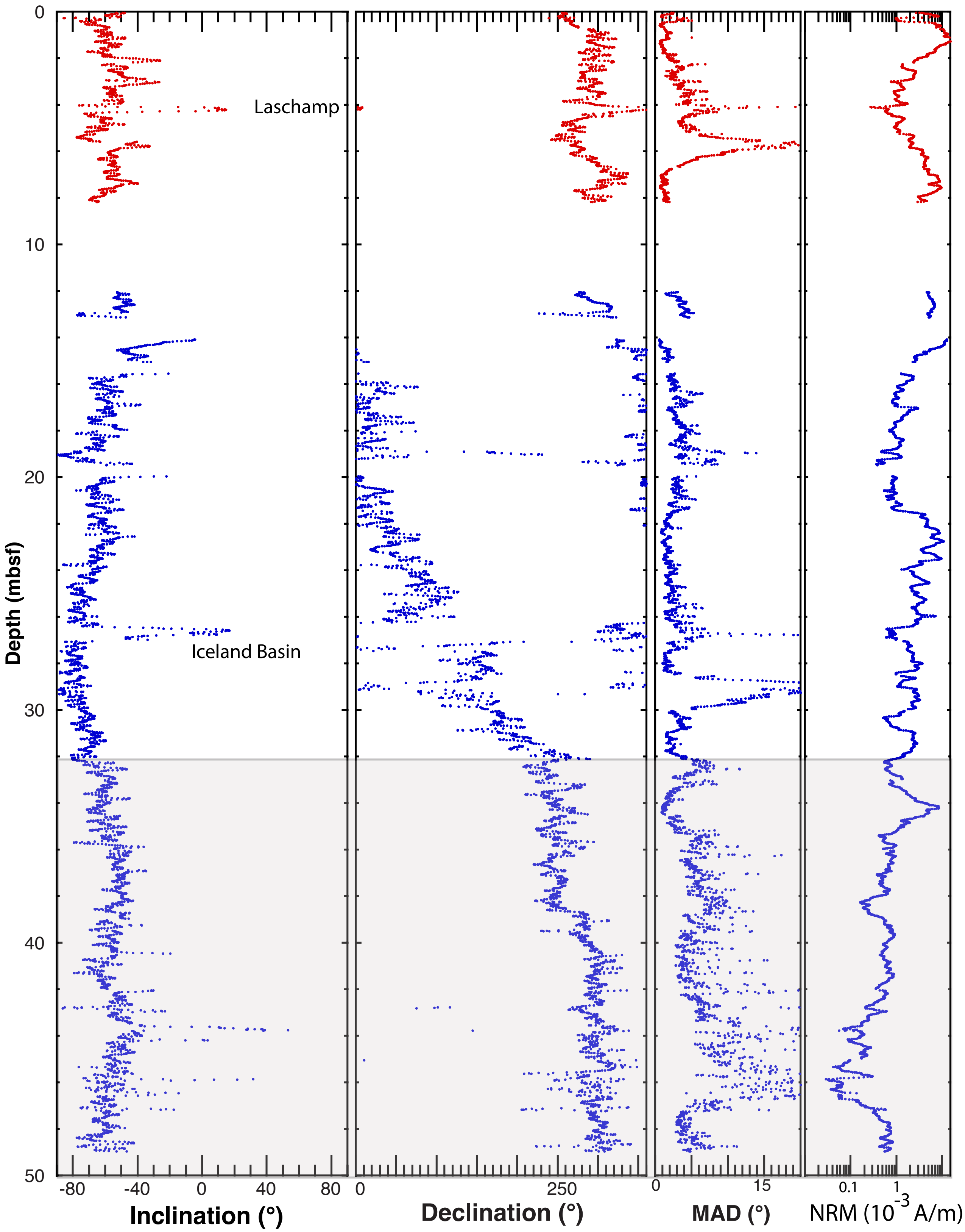

0
10
20
30
40
50
Depth (mbsf)
Laschamp
Iceland Basin
-80
-40
0
40
80
Inclination (°)
0
250
Declination (°)
0
15
MAD (°)
0.1
1
NRM (10^{-3} A/m)

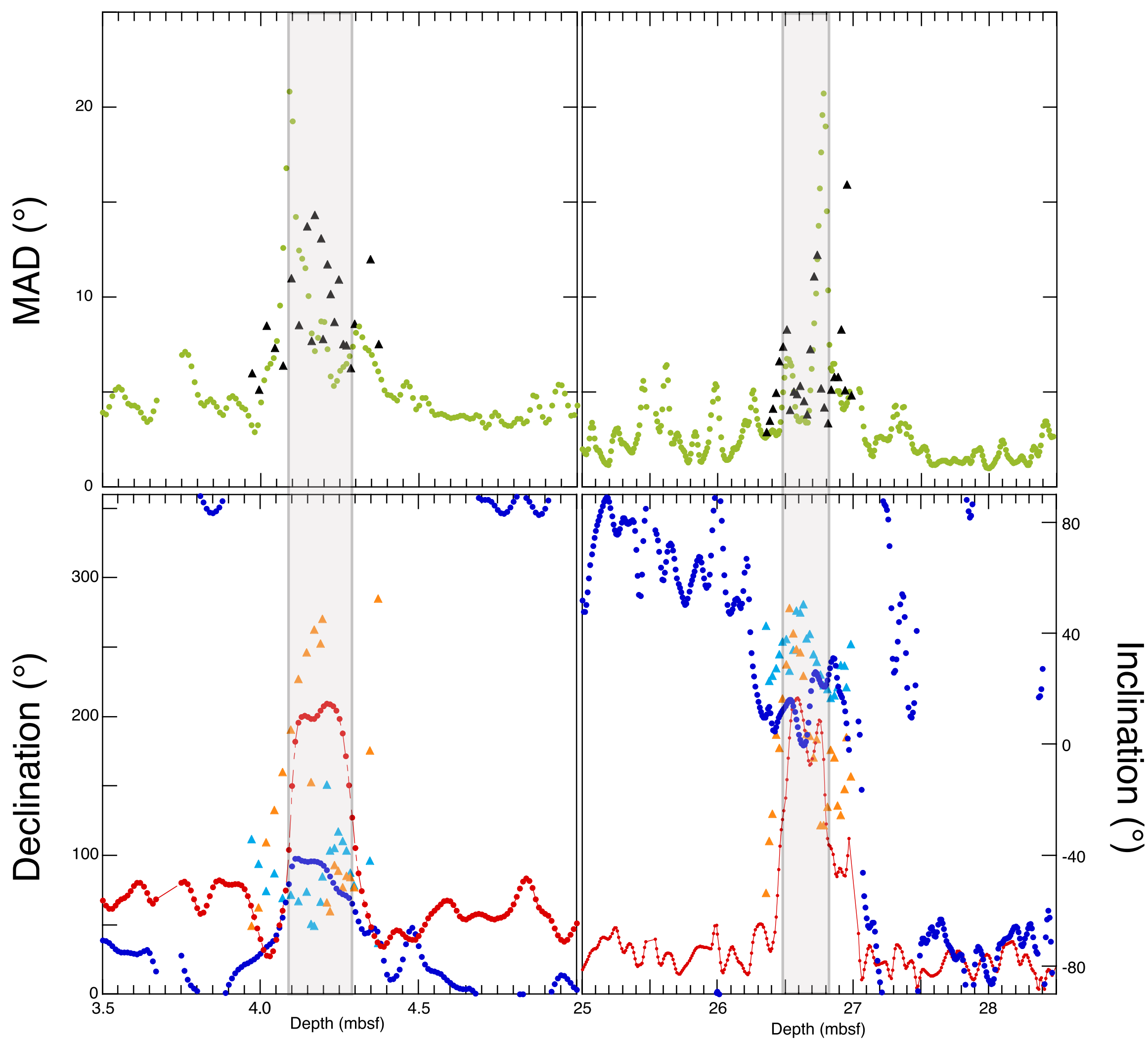

MAD (°)
Declination (°)
Inclination (°)
Depth (mbsf)
Depth (mbsf)

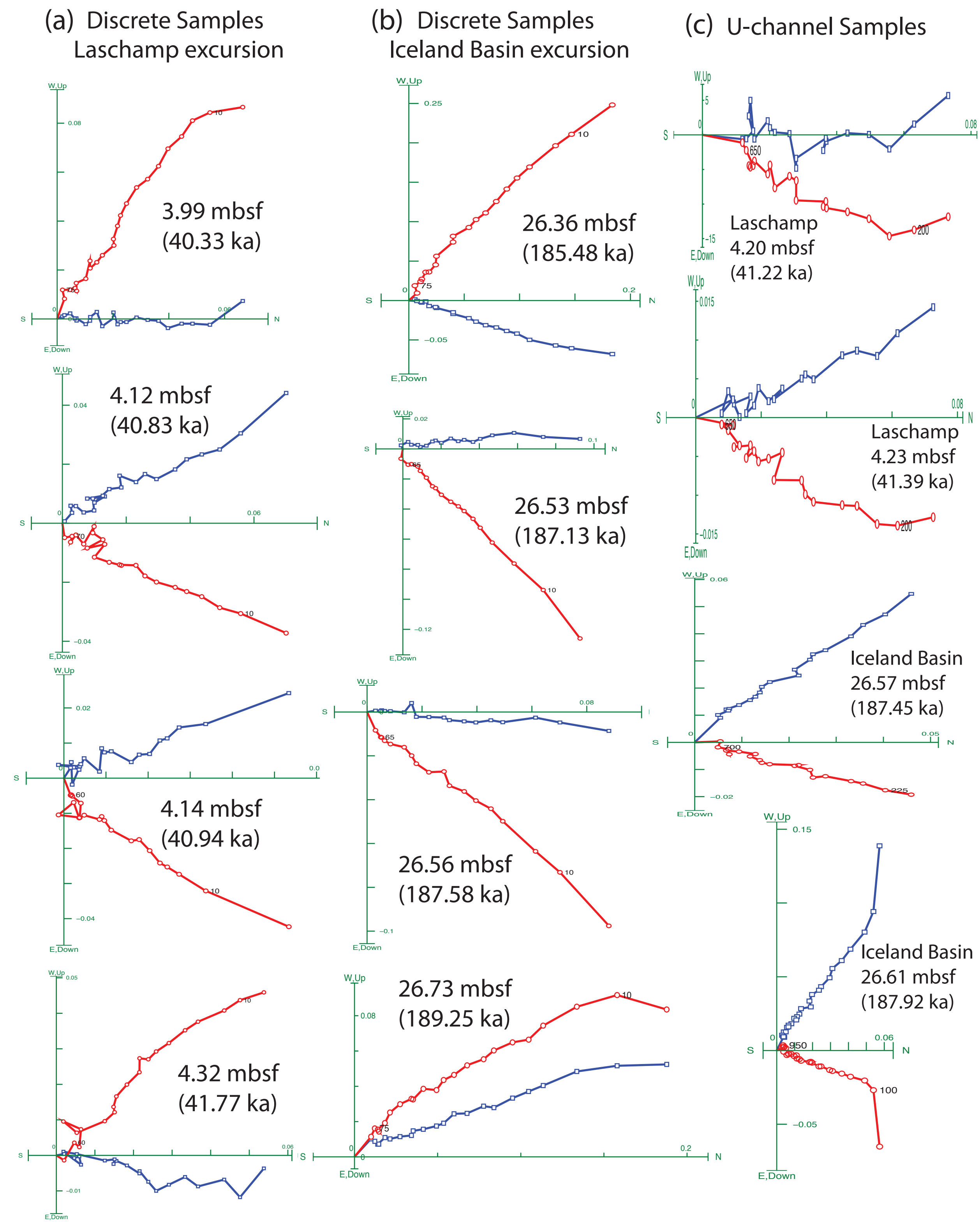

(a) Discrete Samples
Laschamp excursion
(b) Discrete Samples
Iceland Basin excursion
(c) U-channel Samples
3.99 mbsf
(40.33 ka)
4.12 mbsf
(40.83 ka)
4.14 mbsf
(40.94 ka)
4.32 mbsf
(41.77 ka)
26.36 mbsf
(185.48 ka)
26.53 mbsf
(187.13 ka)
26.56 mbsf
(187.58 ka)
26.73 mbsf
(189.25 ka)
Laschamp
4.20 mbsf
(41.22 ka)
Laschamp
4.23 mbsf
(41.39 ka)
Iceland Basin
26.57 mbsf
(187.45 ka)
Iceland Basin
26.61 mbsf
(187.92 ka)
W,Up
E,Down
S
N

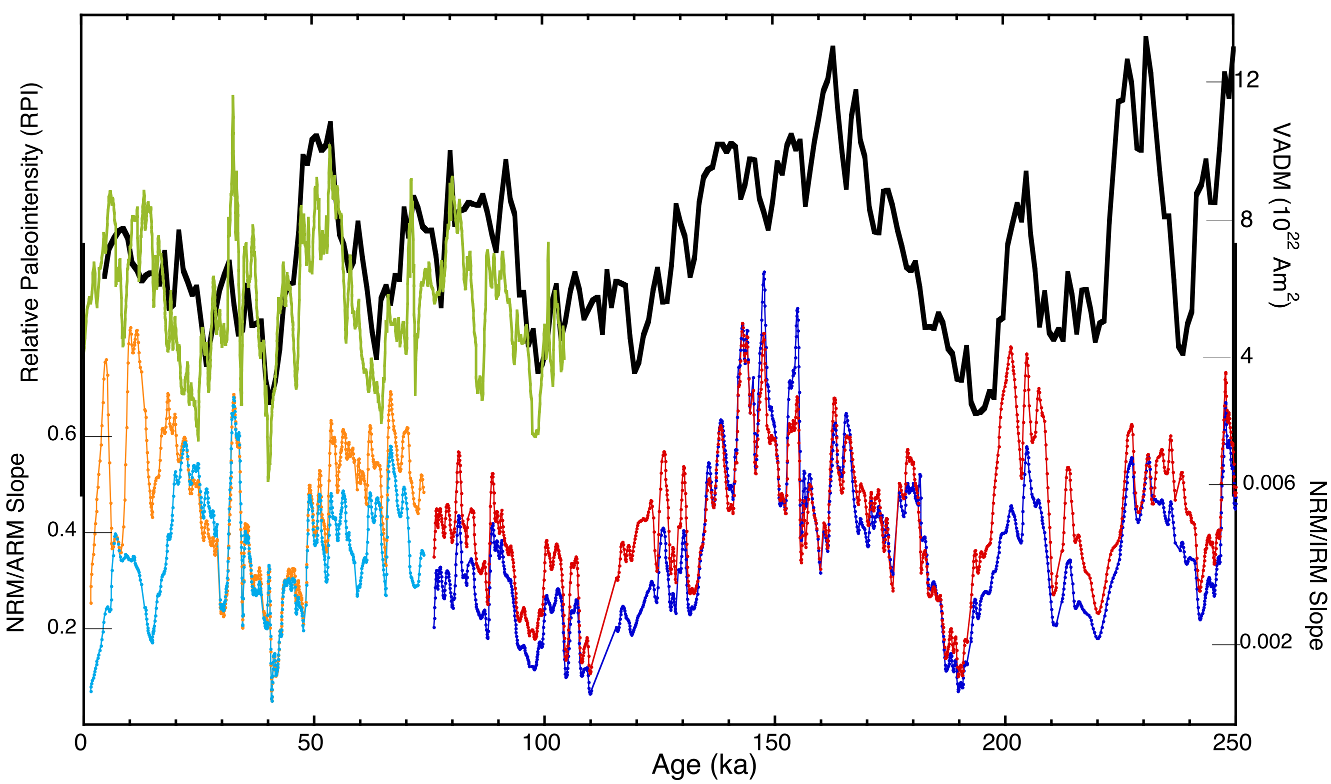

Relative Paleointensity (RPI)
NRM/ARM Slope
0.6
0.4
0.2
VADM (10^{22} Am^2)
12
8
4
NRM/IRM Slope
0.006
0.002
0
50
100
150
200
250
Age (ka)

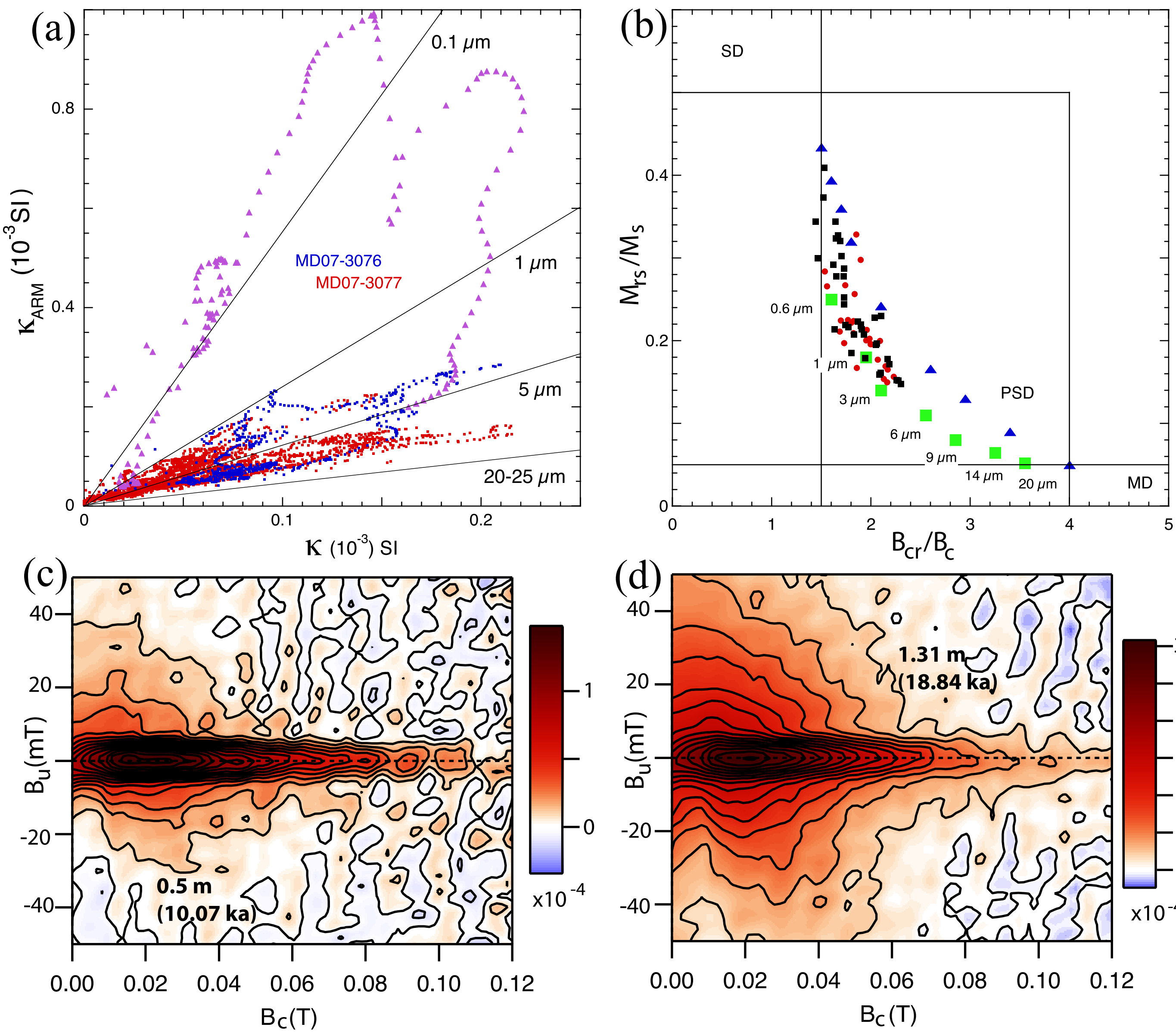
(a)
0.1 μm
1 μm
5 μm
20-25 μm
MD07-3076
MD07-3077
κARM (10-3 SI)
κ (10-3) SI
(b)
SD
PSD
MD
0.6 μm
1 μm
3 μm
6 μm
9 μm
14 μm
20 μm
Mrs/Ms
Bcr/Bc
(c)
0.5 m
(10.07 ka)
Bu(mT)
Bc(T)
x10-4
(d)
1.31 m
(18.84 ka)
Bu(mT)
Bc(T)
x10-4

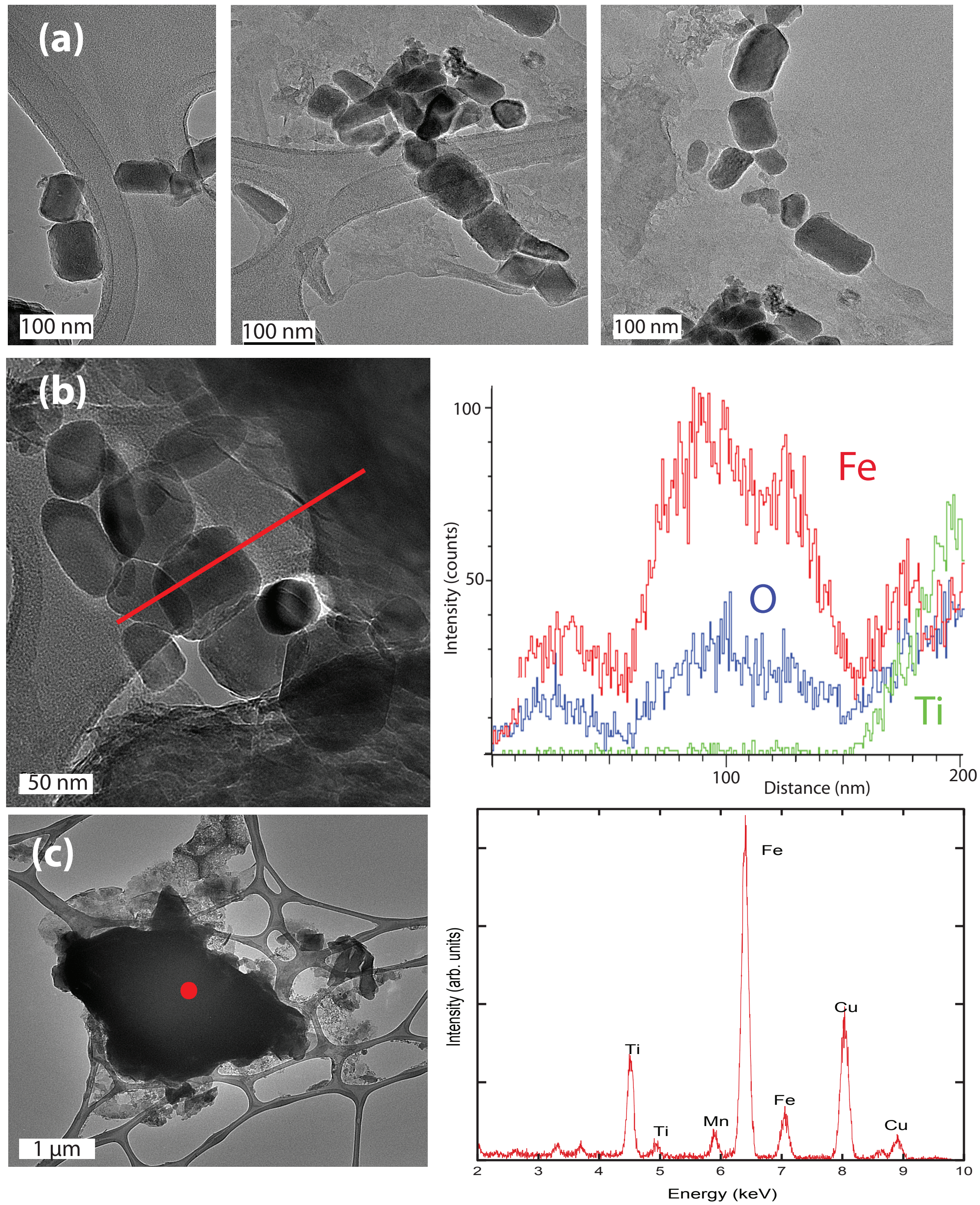
(a)
100 nm
100 nm
100 nm
(b)
50 nm
Intensity (counts)
Distance (nm)
Fe
O
Ti
100
50
100
200
(c)
1 µm
Intensity (arb. units)
Energy (keV)
Fe
Ti
Ti
Mn
Fe
Cu
Cu
2
3
4
5
6
7
8
9
10

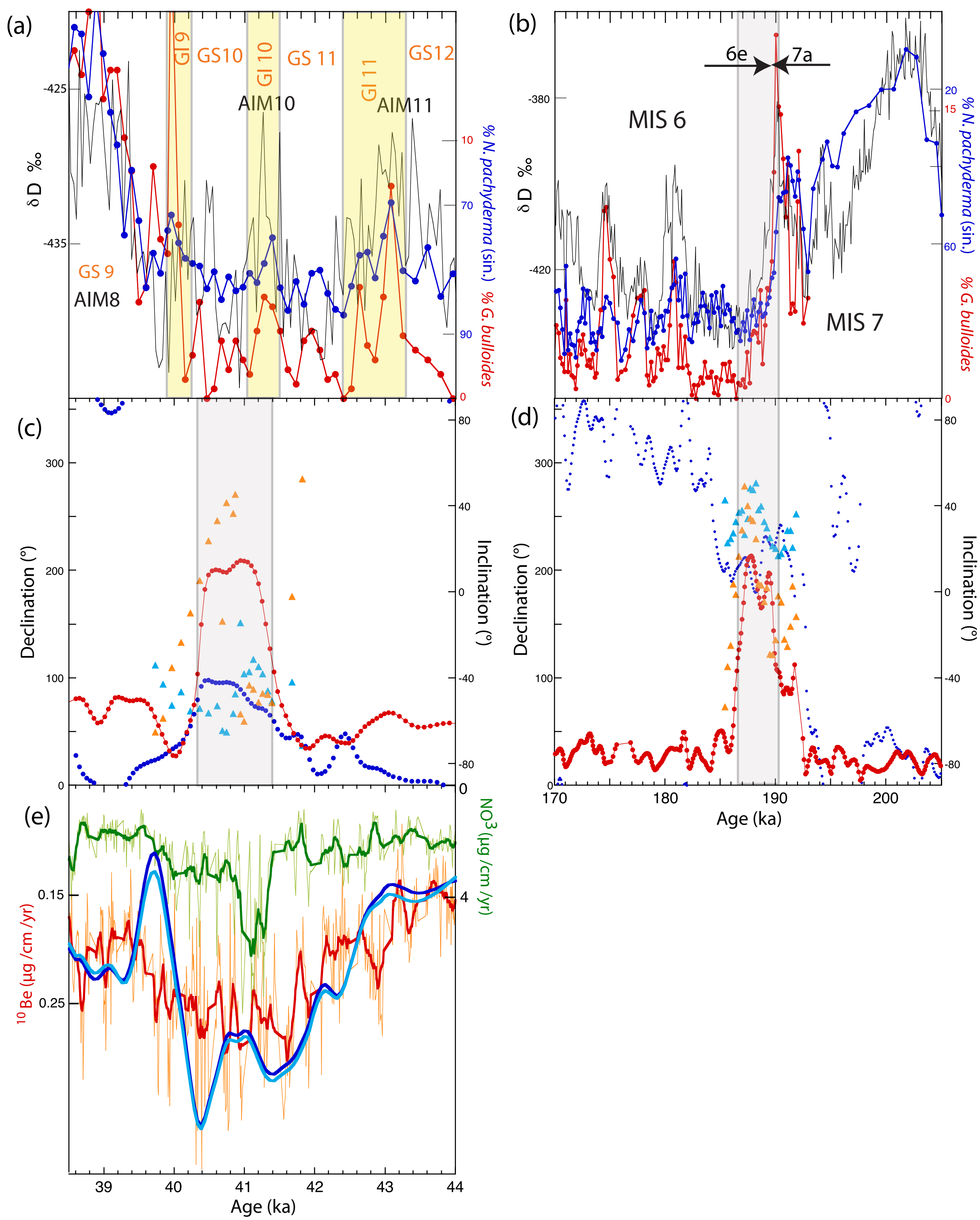

(a)
(b)
(c)
(d)
(e)
GI 9
GS10
GI 10
GS 11
GI 11
GS12
AIM10
AIM11
GS 9
AIM8
δD ‰
% N. pachyderma (sin.)
% G. bulloides
6e
7a
MIS 6
MIS 7
Declination (°)
Inclination (°)
^{10}Be (µg /cm /yr)
NO^3 (µg /cm /yr)
Age (ka)

Highlights

(1) Rare recording of Laschamp and Iceland Basin excursions in the South Atlantic.

(2) Age model links excursions to Antarctic ice core and cosmogenic nuclide flux.

(3) South Atlantic ages consistent with North Atlantic ages for the excursions.

(4) No evidence of global diachroneity of magnetic excursions.

(5) Estimated mid-point ages (durations) are 40.9 ka (1 kyr) and 188 kyr (3.5 kyr).